Available online at www.sciencedirect.com
ScienceDirect
Journal of Power Sources 161 (2006) 250–255
JOURNAL OF POWER SOURCES
www.elsevier.com/locate/jpowsour

Microstructure and electrochemical properties of cathode materials for SOFCs prepared via pulsed laser deposition

Erik Koep*, Chunming Jin, Michael Haluska, Rupak Das, Roger Narayan, Ken Sandhage, Robert Snyder, Meilin Liu

School of Materials Science and Engineering, Georgia Institute of Technology, Atlanta, GA 30332-0245, United States

Received 3 February 2006; received in revised form 21 March 2006; accepted 28 March 2006
Available online 12 July 2006

Abstract

Dense $La_{0.8}Sr_{0.2}MnO_3$ (LSM) and $La_{0.5}Sr_{0.5}CoO_3$ (LSC) films were fabricated via pulsed laser deposition (PLD) on different substrates. The crystal structures of the films were characterized via in situ X-ray diffraction and the in-plane electrical properties by impedance spectroscopy from room temperature to 700 °C. While the ablated films appeared to grow in the perovskite phase with the appropriate electrical properties when the substrate temperature was greater than 500 °C, they were amorphous when the substrate temperature was relatively low. Subsequent annealing of amorphous LSM and LSC films in air induced a rapid phase transformation to the perovskite phase. On silicon substrates, this phase transformation occurred at 450 and 600 °C, respectively.

Keywords: SOFC; Fuel cell; Lanthanum manganate; Cathode; LSM; LSC

1. Introduction

Strontium doped $La_{0.8}Sr_{0.2}MnO_3$ (LSM) and Strontium doped $La_{0.5}Sr_{0.5}CoO_3$ (LSC) have long been recognized as excellent materials for solid state electronic devices [1–4]. The mixed ionic and electronic conductivities of these materials make them ideal choices for electrodes in solid oxide fuel cells [3,5,6] (SOFC) and oxygen sensors [7,8]. Recently, alternative electrolyte materials have shown sufficient oxygen ion conductivity at 500–800 °C, sparking renewed interest in low-temperature SOFC operation [9–11]. Furthermore, in combination with innovative ultra thin film fabrication methods [12,13], SOFC operation at 300–500 °C may be possible.

Dramatically reduced operating temperatures permit a multitude of possible improvements and potential cost reductions. However, in order to achieve high performance at low-temperatures, oxygen reduction kinetics at the cathode must be improved [14]. One step in improving the rate of oxygen reduction at low-temperatures involves the development of a fundamental understanding of the low-temperature behavior of LSM and LSC.

Pulsed laser deposition (PLD) has emerged as an ideal method for growing complex multi-element films, such as LSC and LSM. Due to its unique method of dislodging atoms from the target, PLD provides some distinct advantages unique among thin film techniques. Paramount among these advantages is the capability for stoichiometric material transfer. For deposition techniques based on ions or electrons, the chamber atmosphere greatly influences the film properties and stoichiometry. However, due to the weak interaction of lasers with gaseous species, ambient atmospheres can be used for PLD with very little contamination. When combined with the high heating rates and plasma-induced ablation, stoichiometric transfer of atoms from the target to the substrate can be achieved [15].

PLD has recently demonstrated a unique capability for thin film growth at high or low substrate temperatures [16]. Recently, perovskite films have been successfully developed by PLD through high-temperature deposition or subsequent annealing [17–20]. While the high-temperature behavior is fairly well understood, the low-temperature behavior so far has been neglected. In particular, low-temperature PLD has been shown to be useful for a variety of novel techniques where a high sub-

* Corresponding author. Tel.: +1 404 894 1247; fax: +1 404 894 9140.
E-mail address: gte718w@prism.gatech.edu (E. Koep).

0378-7753/$ – see front matter © 2006 Elsevier B.V. All rights reserved.
doi:10.1016/j.jpowsour.2006.03.060

strate temperature can be particularly damaging [21–23]. Here, we present the characterization and low-temperature behavior of LSM and LSC thin films grown by PLD.

2. Experimental

Thin oxide films of LSC and LSM were prepared via a pulsed laser deposition (PLD) method. A discrete target was developed for each material. The single-phase $La_{0.8}Sr_{0.2}MnO_3$ target was prepared by solid state reaction method. LSM powder was synthesized from a molar ratio of La_2O_3, $SrCO_3$, and Mn_2O_3. The powder mixture was ball milled, pressed isostatically to a pressure of 11 tonnes and calcined at 1150 °C for 5 h. The pellet was then ground and ball milled again to a fine powder. The powder was repressed into a pellet and sintered into its final shape at 1300 °C for 5 h. The LSC target was made from LSC powder purchased from Rhodia. The powder was isostatically pressed to 11 tonnes and fired at 1200 °C for 5 h.

Thin films were deposited on a variety to substrates and under several operating conditions. Silicon (1 0 0), single crystal (1 0 0) yttria stabilized zirconia (YSZ), and polycrystalline tape-cast YSZ were used as substrates. Films were deposited both at room temperature and at 500 °C. Each film type was deposited on all three substrates, yielding a total of six independent samples.

Prior to deposition, the substrates were clamped to the substrate heater and the chamber was evacuated to the prescribed oxygen partial pressure. If necessary, the substrates were brought to 500 °C under vacuum prior to deposition. For deposition, the target was encapsulated in a high vacuum chamber pumped to a base pressure of 1×10^{-4} Torr. The oxygen partial pressure was held constant at 0.1 mTorr in order to minimize the film cracking and surface roughness that may occur at high oxygen partial pressure [24]. A COMPex Model 205 laser from Lambda Physik with a 25 ns pulse duration was used for ablation. The distance between the substrate and the target was 10 cm. The laser was operated at 10 Hz and 353 mJ yielding a typical deposition rate around 2 Å s^{-1}.

A Panalytical X-pert Pro MPD diffractometer with theta–theta geometry was used along with an Anton-Paar HTK1200 high-temperature furnace to perform in situ high-temperature X-ray diffraction on the as-deposited films. Fixed 1/8° incident beam divergence slits were used along with 0.04° incident soller slits and a tube power of 45 kV and 40 mA. An Xcelerator linear detector with an acceptance window of 2.127° 2θ was used in scanning mode. In situ diffraction measurements were taken from 300 to 900 in 50 °C temperature intervals. Each measurement was from 20° to 60° 2θ using a 0.216° 2θ s^{-1} scan rate. The samples were heated at 60 °C min^{-1} under static air. Temperature calibration was performed using the NIST DTA standards $KClO_4$ (Tt 299.5 °C) and Ag_2SO_4 (Tt 430 °C) and showed an approximately +10 °C temperature difference.

For electrical measurements, interdigitated arrays of 10 platinum electrodes each were fabricated on insulating quartz substrates. The electrodes were lithographically patterned in order to ensure a constant spacing of 20 μm between alternating electrodes. For simplicity, the details of the photolithographic process have been presented elsewhere [23]. Thin LSM and LSC films were then ablated directly onto the prepared substrate. Electrical contacts were attached to the alternate arrays and impedance spectroscopy was used to analyze the electrical response. Fig. 1a presents a schematic of the electrode layout used for impedance measurements. Fig. 1b is a low magnification image of the LSC film overlaid onto the interdigitated platinum electrode.

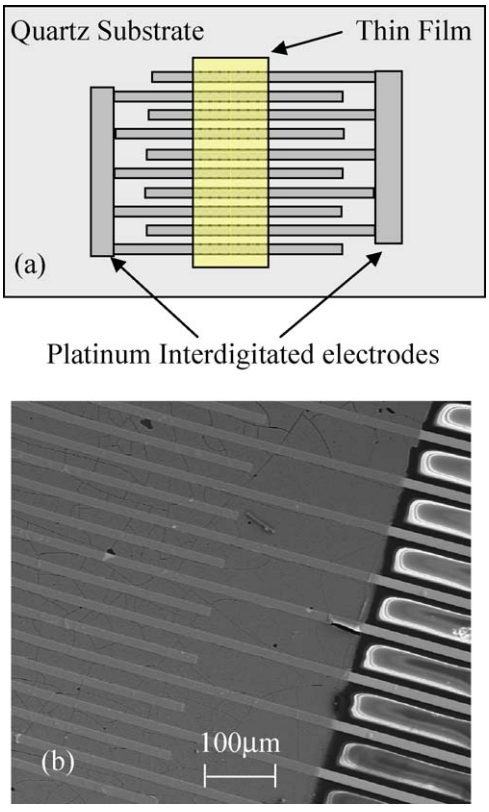

Fig. 1. Schematic (a) and SEM micrograph (b) of the electrode set-up for electrochemical impedance testing prior to testing, the electrodes were patterned on a quartz substrate and taped to prevent deposition on the electrode contacts. The thin LSM and LSC films were then grown over the top of the substrate in the prescribed area. Each 20 μm wide electrode strip is separated by a 20 μm gap. LSM and LSC film thickness were 700 and 300 nm, respectively.

Each sample was run individually at constant temperature in 100 °C increments ranging from 100 to 700 °C. A Solatron 1255 frequency response analyzer connected through a Solatron 1287 electrochemical interface collected impedance data over a range from 100 kHz to 0.01 Hz. A Tencor Alpha Step Profilometer was used to independently verify the thickness of the LSC and LSM films. Impedance results were characterized through a simple model to calculate the conductivity values of the films.

3. Results and discussion

Fig. 2 displays an SEM micrograph of the as-tested thin LSM film. All films appeared completely dense and pore-free. Additionally, the films showed good adhesion to the substrate with no instances of delamination. Figs. 3 and 4 show top down views of the LSM and LSC films before and after testing. Figs. 3a and 4a

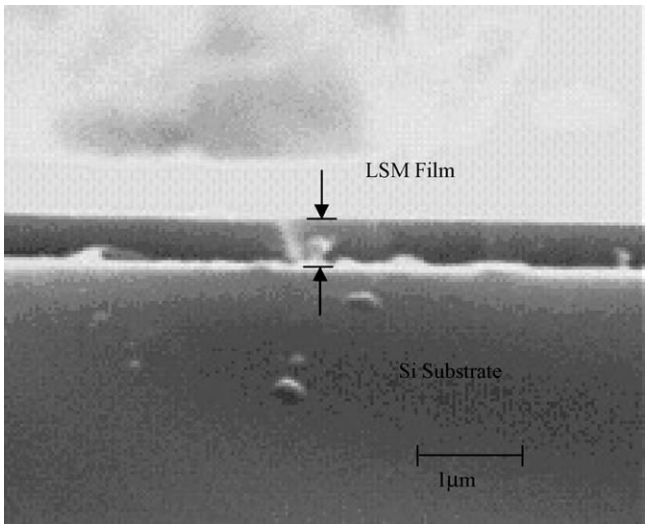

Fig. 2. SEM cross-sectional micrograph of a thin dense LSM film approximately 0.6 μm in thickness supported on a quartz substrate. This film was fired up to 800 °C and is shown in the final state.

display SEM micrographs of the as prepared LSM and LSC films, respectively. The amorphous films display a unique lack of any distinguishable features and, for the LSC film, the structure of the underlying electrode can be easily recognized. By contrast, Figs. 3b and 4b display SEM micrographs of LSM and LSC films after annealing in air up to 900 °C for 30 min. The small grain features and some minor cracking on the surface of the annealed films readily contrast the featureless characteristics of the amorphous films.

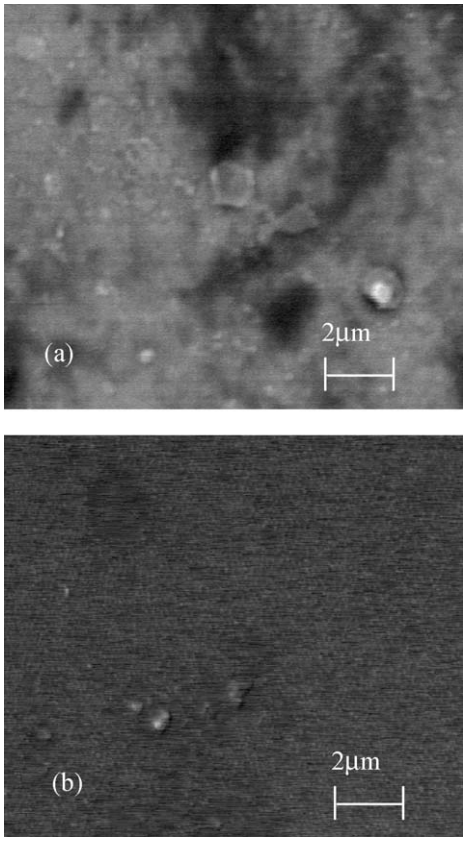

Fig. 3. (a and b) SEM micrographs of thin film LSM before (a) and after firing (b). (a) Displays the characteristics of the as prepared LSM films. No significant grains can be discerned on the films, a trait characteristic of amorphous films. (b) Exhibits the film after high-temperature testing. Limited grain growth can be seen.

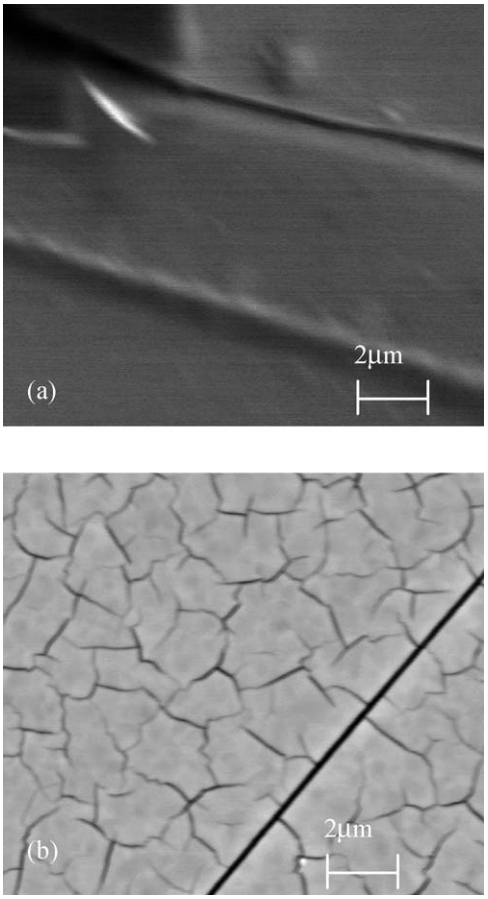

Fig. 4. (a and b) SEM micrographs of thin film LSC before (a) and after (b) firing. (a) Displays the characteristics of the as prepared LSC films. No significant grains can be discerned on the films, a trait characteristic of amorphous films. (b) Exhibits the film after high-temperature testing. Limited grain growth can be seen.

Shown in Fig. 5 are a series of temperature-dependent XRD diffraction patterns of a thin LSM film deposited on a silicon (1 0 0) substrate at room temperature. The low-angle hump apparent in the XRD patterns acquired at low-temperatures (300–400 °C) is an indication that the LSM film was amorphous. The phase transition from an amorphous state to the orthorhombic phase (PDF #53–57) can be seen to occur between 400 and 450 °C. In direct comparison, the LSM films deposited at a substrate temperature of 500 °C were recorded in the orthorhombic phase initially. The initial and final film phases did not depend on the choice of substrate. However, the devitrification temperatures for thin films on both the single crystal YSZ and the polycrystalline YSZ were recorded between 500 and 550 °C, roughly 100 °C higher than that for silicon.

Fig. 6 presents the temperature-dependent XRD patterns of a thin LSC film on a silicon (1 0 0) substrate deposited at room temperature. The low-angle hump associated with amorphous film is less apparent in the XRD patterns acquired at

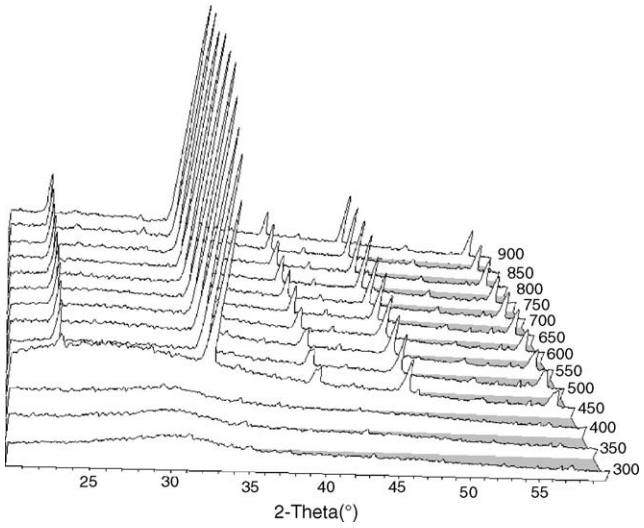

Fig. 5. Temperature-dependant XRD scan on thin film LSM on (1 0 0) silicon intensity is plotted as a function of 2θ on the *X*-axis and temperature in celsius on the *Y*-axis. The phase change from amorphous to the perovskite phase occurs between 400 and 450 °C.

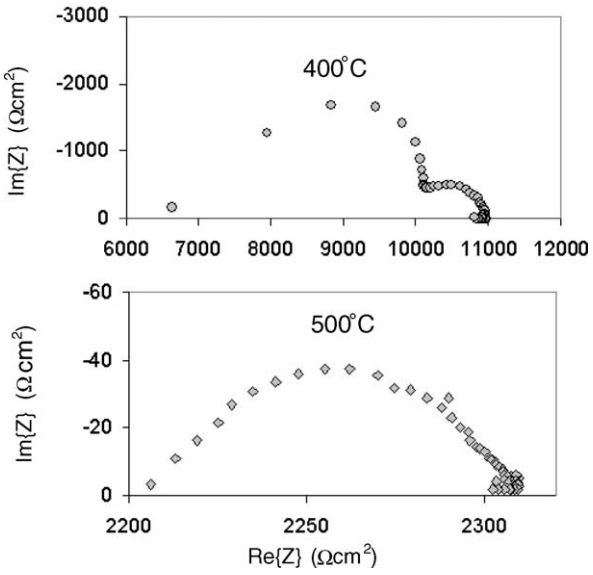

Fig. 7. A typical impedance spectra of an LSM film measured in air at 400 and 500 °C, respectively. The film was grown via pulsed laser deposition at room temperature.

low-temperatures (300–400 °C). Additionally, a minor impurity phase can be seen below the 600 °C transition temperature. The phase transition from a predominately amorphous state to the rhombohedral phase (PDF #48–122) can be clearly seen between 550 and 600 °C for LSC. Again, in direct comparison, the LSC films deposited at 500 °C were recorded in the rhombohedral phase initially. For a second time, the initial and final film phases did not depend on the choice of substrate, although the devitrification temperature for thin films on both the single crystal YSZ and the polycrystalline YSZ was recorded roughly 100 °C higher than that for silicon. For the YSZ substrates, the phase transition occurred between 650 and 700 °C.

Above 900 °C, degradation of the LSC film on silicon becomes evident. A decrease in the peak heights of the rhombohedral $La_{0.5}Sr_{0.5}CoO_3$ phase in conjunction with the appearance of a second La_2CoO_4 phase (PDF #34–1296) leads to the conclusion that decomposition was occurring in this instance. This decomposition was not seen with LSC films on either single crystal YSZ or polycrystalline YSZ substrates.

Repeat analysis of the phase change as a function of time reflected the relative time-independence of the phase change. Several temperature-independent scans were performed at 430 °C for LSM and 580 °C for LSC in hopes of observing the phase change as a function of time. Unfortunately, all phase changes occurred too quickly to be measured with our equipment. In both cases, the phase changes occurred below the 9-s window necessary for time-dependant measurements; as a result, we were unable to obtain any useful information on the kinetics of the phase transformation.

Shown in Figs. 7 and 8 are typical impedance spectra for LSM and LSC thin films prepared by PLD at low-temperatures. The bulk resistance (or the in-plane sheet resistance) of the films was determined from the intercept with the real axis at high frequencies. Meanwhile the interfacial polarization resistance between the films and the Pt electrodes was determined from

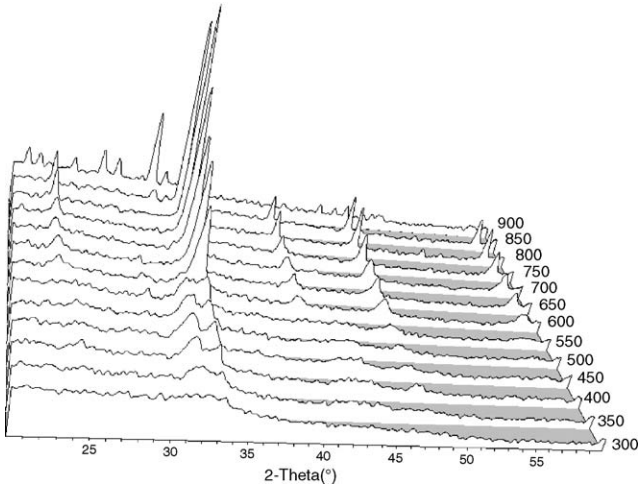

Fig. 6. Time-dependant XRD scan of thin film LSC on (1 0 0) silicon. The phase change between 550 and 600 °C can be clearly discerned.

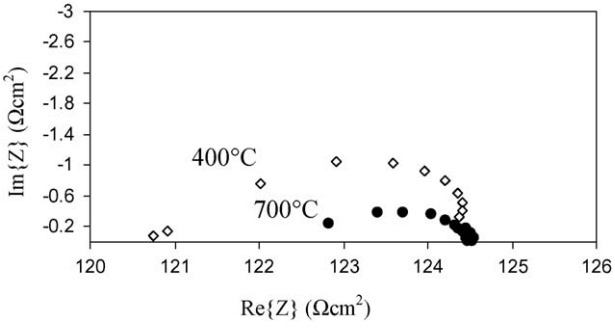

Fig. 8. A typical impedance spectra of an LSC film measured in air at 400 and 700 °C, respectively. The film was grown via pulsed laser deposition at room temperature.

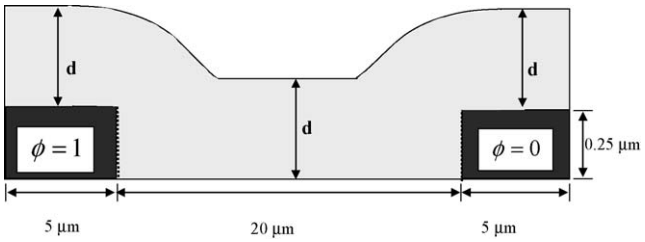

Fig. 9. Schematic of the cross-sectional conductivity model A vertical sliced-cross-section was taken from the electrode array in order to portray the model domain. The black boundaries were assigned to represent the platinum current collectors. The thickness of the LSM or LSC film was defined as *d*, while the platinum current collectors were held constant at a thickness of 0.25 μm.

the diameter of the small impedance loop. All of the amorphous films exhibited this type of behavior.

Conductivity values were calculated via a finite element model developed for the specific electrode geometry schematically shown in Fig. 9. The electrical potentials of the two platinum electrodes were assumed to be 0 and 1 V, respectively, and each platinum electrode was assumed to be equipotential. On the other hand, since the quartz substrate used for this experiment has extremely low conductivity relative to both the platinum electrodes and the thin cathode films, current through the substrate was neglected. The thickness of the film was designated as *d* and chosen in accordance with the actual thickness of the electrode films. The thickness of the LSC and LSM films were measured to be 0.2 and 0.7 μm, respectively, as verified by profilometry.

The Laplace equation, $\nabla^2\phi = 0$, was solved in the whole domain (LSM or LSC films) as the only constitutive equation. All the boundaries were kept insulated with the obvious exception of the interfaces of the two platinum electrodes with the thin film of LSM or LSC. Ohm's law was then used to calculate the effective conductivity of the media as follows:

$$I = \iint_{\text{Area}} -\sigma_{\text{eff}} \frac{\delta\phi}{\delta y}$$

where I is the total current flowing through the sample film between the two platinum electrodes (or the interfaces between the platinum electrodes and the LSM or LSC films) and $\delta\phi/\delta y$ is the electrical potential gradient on an interface between a platinum electrode and the LSM or LSC film. The surface integration was carried out over the entire interface between the platinum electrode and the LSM or LSC film. For each applied voltage, the total current passing through the sample film was experimentally measured whereas the potential distribution at each point on the interface were calculated using finite element modeling (Femlab version 3.1).

The temperature dependant behavior of both LSM and LSC is displayed in Fig. 10. For LSM films of 0.7 μm in thickness, the calculated conductivity was approximately 21 S cm^{-1} at 700 °C. The calculated conductivity for LSC was approximately 172 S cm^{-1} at 700 °C. For both the LSM and LSC, conductivity values agreed well with those reported in literature [25].

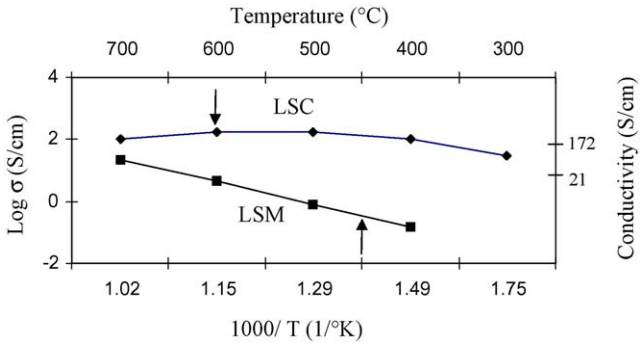

Fig. 10. Plot of log conductivity vs. 1/temperature for both LSM and LSC. The transition points between the amorphous and crystalline phases are 450 and 600 °C and are indicated by arrows. It is important to note that the electronic behavior is consistent throughout both the crystalline and amorphous phases.

4. Conclusion

Dense and uniform films of mixed conducting materials, LSM and LSC, have been fabricated by PLD. The structures and properties of the PLD films vary with deposition temperature and substrate material, as revealed using electron microscopy, impedance spectroscopy, and temperature dependant X-ray diffraction.

Deposition of LSM and LSC above 500 °C resulted in thin dense films in the orthorhombic and rhombohedral phases, respectively. The stoichiometry of the films was the same as the target materials and there were no phase changes upon annealing. Crystalline films generated by PLD displayed anticipated conductivities.

In contrast, low-temperature deposition yielded amorphous films with the correct stoichiometry. Upon annealing, both LSM and LSC amorphous films transformed rapidly to the crystalline phase. The temperature for this rapid phase transformation was 550 °C for LSM and 700 °C for LSC film on a YSZ substrate, but at a temperature roughly 100 °C cooler on silicon substrates. Impedance spectroscopy studies indicate that the electrical properties of both LSM and LSC films appear similar to those reported in the literature and the conductivity values at 700 °C for LSM and LSC are 21 and 172 S cm^{-1}, respectively.

It is noted that the temperatures at which the PLD films transformed to the perovskite phase are significantly below the firing temperatures required for more traditional methods of film preparation. Thus, PLD opens possibilities for unique fabrication of useful phases without high-temperature annealing and thus holds promise for low-temperature fabrication of SOFCs.

Acknowledgement

This work was supported by DoE-NETL SECA Core Technology Program (Grant no. DE-FC26-02NT41572).

References

[1] S. Skinner, Int. J. Inorg. Mater. 3 (2001) 113.
[2] M. Morgensen, S. Skaarup, Sol. State Ion. 86–88 (1996) 1151.
[3] B.C.H. Steele, Sol. State Ion. 86–88 (1996) 1223.

[4] A.J. McEvoy, Sol. State Ion. 132 (2000) 159.
[5] N.Q. Minh, Ceram. Fuel Cells J. Am. Ceram. Soc. 76 (1993) 563.
[6] O. Yamamoto, Y. Takeda, R. Kanno, M. Noda, Sol. State Ion. 22 (1987) 241.
[7] P. Fedtke, M. Wienecke, M. Bunescu, T. Barfels, K. Deistung, M. Pietrzak, J. Sol. State Electrochem. 8 (2004) 626.
[8] J. Ramirez-Salgado, P. Fabry, Sol. State Ion. 158 (2003) 297.
[9] R. Doshi, V.L. Richards, J.D. Carter, X. Wang, M. Krumplet, J. Electrochem. Soc. 146 (1999) 1273.
[10] H. Yahiro, Y. Baba, K. Eguchi, H. Arau, J. Electrochem. Soc. 135 (1988) 2077.
[11] B.C.H. Steele, Sol. State Ion. 129 (2000) 95.
[12] J. Fleig, H.L. Tuller, J. Maier, Sol. State Ion. 174 (2004) 261.
[13] X. Chen, N.J. Wu, L. Smith, A. Ignatiev, Appl. Phys. Lett. 14 (2004) 2700.
[14] C. Xia, M. Liu, Sol. State Ion. 144 (2001) 249.
[15] D. Chrisey, G. Hubler, Pulsed Laser Deposition of Thin Films, John Wiley and Sons, 1994.
[16] N.Q. Minh, T. Takahashi, Science and Technology of Ceramic Fuel Cells, Elsevier Science, 1995.
[17] N. Imanishi, T. Matsumura, Y. Sumiya, K. Yoshimura, A. Hirano, Y. Takeda, D. Mori, R. Kanno, Sol. State Ion. 174 (2004) 245.
[18] A. Tiwari, A. Chug, C. Jin, D. Kumar, J. Narayan, Sol. State Commun. 121 (2002) 679.
[19] Y. Chen, L. Sun, Y. Pan, Y. Tao, Z. Liu, N. Ming, Mater. Lett. 27 (1996) 139.
[20] A. Endo, H. Fukunaga, C. Wen, K. Yamada, Sol. State Ion. 135 (2000) 353.
[21] M. Alexe, C. Harnagea, D. Hesse, J. Electroceram. 12 (2004) 69.
[22] C.R. Martin, I.A. Aksay, J. Electroceram. 12 (2004) 53.
[23] E. Koep, C. Compson, M. Liu, Z. Zhou, Sol. State Ion. 176 (2005) 1.
[24] Y. Yao, S.G. Lu, H. Chen, J. Zhai, K.H. Wong, J. Appl. Phys. 96 (1) (2004) 569.
[25] H. Lee, Mater. Chem. Phys. 77 (2002) 639–646.